



Original article

Enantiopure bifunctional chelators for copper radiopharmaceuticals – Does chirality matter in radiotracer design?☆

Ajay N. Singh^{a,b,1}, Marianna Dakanali^{a,1}, Guiyang Hao^a, Saleh Ramezani^a, Amit Kumar^a, Xiankai Sun^{a,c,*}^a Department of Radiology, The University of Texas Southwestern Medical Center, Dallas, TX, USA^b Department of Basic Science, Appalachian College of Pharmacy, Oakwood, VA, USA^c Department of Advanced Imaging Research Center, The University of Texas Southwestern Medical Center, Dallas, TX, USA

ARTICLE INFO

Article history:

Received 18 January 2014

Received in revised form

22 April 2014

Accepted 23 April 2014

Available online 25 April 2014

Keywords:

Molecular imaging

Positron emission tomography

Integrin $\alpha_v\beta_3$

Copper-64

Bifunctional chelator (BFC)

Imaging

Diagnosis

Prognosis

ABSTRACT

It is well recognized that carbon chirality plays a critical role in the design of drug molecules. However, very little information is available regarding the effect of stereoisomerism of macrocyclic bifunctional chelators (BFC) on biological behaviors of the corresponding radiopharmaceuticals. To evaluate such effects, three enantiopure stereoisomers of a copper radiopharmaceutical BFC bearing two chiral carbon atoms were synthesized in forms of R,R-, S,S-, and R,S-. Their corresponding peptide conjugates were prepared by coupling with a model peptide sequence, c(RGDyK), which targets the $\alpha_v\beta_3$ integrin for *in vitro* and *in vivo* evaluation of their biological behaviors as compared to the racemic conjugate. Despite the chirality differences, all the conjugates showed a similar *in vitro* binding affinity profile to the $\alpha_v\beta_3$ integrin (106, 108, 85 and 100 nM for rac-H₂-1, RR-H₂-1, SS-H₂-1, and RS-H₂-1 respectively with all *p* values > 0.05) and a similar level of *in vivo* tumor uptake (2.72 ± 0.45 , 2.60 ± 0.52 , 2.45 ± 0.48 and 2.88 ± 0.59 for rac-⁶⁴Cu-1, RR-⁶⁴Cu-1, SS-⁶⁴Cu-1, and RS-⁶⁴Cu-1 at 1 h p.i. respectively). Furthermore, they demonstrated a nearly identical biodistribution pattern in major organs (e.g. 2.07 ± 0.21 , 2.13 ± 0.58 , 1.70 ± 0.20 and 1.90 ± 0.46 %ID/g at 24 h p.i. in liver for rac-⁶⁴Cu-1, RR-⁶⁴Cu-1, SS-⁶⁴Cu-1, and RS-⁶⁴Cu-1 respectively; 1.80 ± 0.46 , 2.30 ± 1.49 , 1.73 ± 0.31 and 2.23 ± 0.71 at 24 h p.i. in kidneys for rac-⁶⁴Cu-1, RR-⁶⁴Cu-1, SS-⁶⁴Cu-1, and RS-⁶⁴Cu-1 respectively). Therefore we conclude that the chirality of BFC plays a negligible role in $\alpha_v\beta_3$ -targeted copper radiopharmaceuticals. However, we believe it is still worthwhile to consider the chirality effects of BFCs on other targeted imaging or therapeutic agents.

© 2014 Elsevier Masson SAS. All rights reserved.

1. Introduction

Positron emission tomography (PET) is routinely used in clinical and preclinical settings for diagnostic or prognostic imaging of cancer or other diseases [1–5]. The success of PET lies in its high sensitivity and specificity to detect physiological changes at cellular or molecular level. Combined with computed tomography (CT), dual-modal PET/CT imaging provides both molecular changes and

detailed anatomical information for a better diagnosis. Currently, ¹⁸F ($t_{1/2} = 109$ min) and ¹¹C ($t_{1/2} = 20.3$ min) are the most commonly used PET radionuclides for the development of PET imaging probes. However, their short half-lives limit their applications mainly in small organic or biological molecules. Recently, ⁶⁴Cu ($t_{1/2} = 12.7$ h; $E_{\beta^+ \text{ max}} = 0.653$ MeV, 17.4%), a non-standard PET radionuclide, has drawn considerable attention in the community of PET due to its low positron energy, commercial availability, and reasonably long decay half-life [6,7]. More importantly, the well-established coordination chemistry of copper potentially enables a rapid translation from bench-top science to clinical practice of copper radiopharmaceuticals with a variety of imaging or radio-therapeutic applications involving peptides, antibodies or their fragments, and nanoparticles [8–10].

The stability of the metal complex moiety is of critical importance in the design of a metal radiopharmaceutical. In the past decade, we and other groups had research focused on a cross-

☆ Grant support: This work was partially supported by the Prostate Cancer Research Program of the United States Army Medical Research and Materiel Command (W81XWH-08-1-0305 and W81XWH-12-1-0336). The authors acknowledge the generous support of a private donor that allowed the purchase of the Siemens Inveon PET-CT Multi-modality System.

* Corresponding author. University of Texas Southwestern Medical Center, 5323 Harry Hines Blvd, Dallas, TX 75390-8542, USA.

E-mail address: Xiankai.Sun@UTSouthwestern.edu (X. Sun).

¹ Authors contributed to this work equally.

bridged tetraazamacrocyclic chelator, CB-TE2A [4,11-bis-(carbo-*tert*-butoxymethyl)-1,4,8,11-tetraazabicyclo[6.6.2]hexadecane] for the development of novel copper radiopharmaceuticals because CB-TE2A forms one of the most stable complexes with Cu(II), which is more resistant to reductive metal loss than are other tetraazamacrocyclic complexes [11,12]. The high *in vivo* stability of Cu(II)-CB-TE2A complex arises from the perfect match of Cu(II) and the cavity size formed by the pre-organized CB-cyclam ligand [11,13]. In this hexa coordinated complex, Cu(II) is completely encapsulated in the CB-cyclam cavity by four coordinating nitrogen atoms and two carboxylate oxygen atoms. However, once a pendent carboxylate arm of the CB-TE2A is converted to amide during vector conjugation, the stability of the Cu(II)-CB-TE2A will be compromised and the metal moiety become positively charged, which could be detrimental to the biological behavior of the copper radiopharmaceuticals. To avoid this problem, we have recently reported a novel bifunctional chelating (BFC) scaffold based on the CB-TE2A core [10]. The designed BFC scaffold, CB-TE2GA (Fig. 1), utilizes an orthogonally protected glutaric heterodiester as the coordinating side arm. The choice of this side arm allows selective deprotection of the peripheral carboxylates for conjugation with targeting molecules, while the inner carboxylates can be preserved for ^{64}Cu complexation. We reported that the imaging probe so designed (rac- ^{64}Cu -1) indeed showed high *in vivo* stability and enhanced tumor uptake due to the multivalent effect [10].

However, our reported BFC scaffold, CB-TE2GA, bears two chiral carbon atoms in the glutaric acid side arm, which can give rise to three potential stereoisomers [14,15]. When targeting molecules are attached to the side arms, the chirality difference may lead to different spatial dispositions of the targeting moieties depending on the chirality of the side arms, which can potentially impact their binding affinities to the target receptors.

To evaluate the role of chiral BFC in the properties of copper radiopharmaceuticals, we synthesized CB-TE2GA in three enantiopure forms (RR-8, SS-8, RS-8) starting from the enantiopure side arm precursors, namely R- and S-5-benzyl 1-(*tert*-butyl) 2-((methylsulfonyl)oxy)pentadioate (R-6, S-6). The synthesized BFCs, RR-8, SS-8, and RS-8, were conjugated with an $\alpha_v\beta_3$ integrin specific peptide, c(RGDyK), to provide enantiopure peptide conjugates (RR-H₂-1, SS-H₂-1, RS-H₂-1), respectively. When labeled with ^{64}Cu , the peptide conjugates were evaluated by *in vitro* binding assay, PET/CT imaging, and imaging-derived biodistribution profiles in tumor-bearing mice. The racemic conjugate was used as the control for comparative evaluation.

2. Results

2.1. Synthesis

The synthesis of enantiopure RR-H₂-1, SS-H₂-1, and RS-H₂-1 was achieved in three steps; i) synthesis of the chiral side arms, S-6 and R-6 ii) synthesis of the BFC scaffolds, RR-8, SS-8, and RS-8, and iii) conjugation of two molecules of c(RGDyK) on to the BFCs (Schemes 1–3). The synthesis of the chiral side arms, S-6 and R-6, started from L- and D-glutamic acid, respectively. Following a reported procedure [16,17], L- or D-glutamic acid was converted to S- or R-2 respectively, via diazotization using sodium nitrite (NaNO_2) in the presence of excess HCl in 78% yield. The stereoselectivity of the conversion of L-glutamic acid to S-2 depends critically on both the rate of the addition of the aqueous NaNO_2 solution to the acidic L-glutamic acid solution and on the reaction temperature that must be maintained between 0 and 5 °C during the addition [17]. The synthesis of S-2 uses the stereoselectivity of the deamination reaction, which is known to proceed with complete retention of the configuration [16]. The *t*Bu-protected ester S-3 was synthesized in 55% yield using a standard esterification procedure, namely 4-dimethylaminopyridine (DMAP) and *N,N'*-dicyclohexylcarbodiimide (DCC) in tetrahydrofuran (THF). Unlike the reported procedure where S-3 was synthesized from the acid chloride of S-2, the DMAP/DCC directed esterification was easy to handle and the product, lactone S-3, could be purified and obtained at gram scale. The obtained S-3 was then hydrolyzed using one equivalent of 1 N KOH to provide the potassium salt of S-4. A small sample of the above synthesized salt was treated with 3 N HCl to yield the corresponding acid in 60% yield for purification and characterization purposes. The carboxylate salt of S-4 was alkylated with benzyl bromide (BnBr) in dimethylformamide (DMF) to afford the crude S-5, an orthogonally protected diester. Purification of crude S-5 using column chromatography yielded the pure product in 52% yield. The secondary alcohol of S-5 was then converted to the corresponding mesylate as a leaving group to provide S-6 in quantitative yield. Mesylate was chosen as the leaving group based on the fact that it is stable in aqueous workup at room temperature and the controlled alkylation of CB-cyclam by $\text{S}_{\text{N}}2$ reaction affords the complete inversion of stereochemistry of the product. Dialkylation of CB-cyclam was carried out by adding the mesylated S-6 or R-6, to a suspension of a half equivalent of CB-cyclam in acetonitrile preheated to 50 °C in the presence of potassium carbonate. The orthogonally protected diester, RR-7 or SS-7, was obtained in 52%

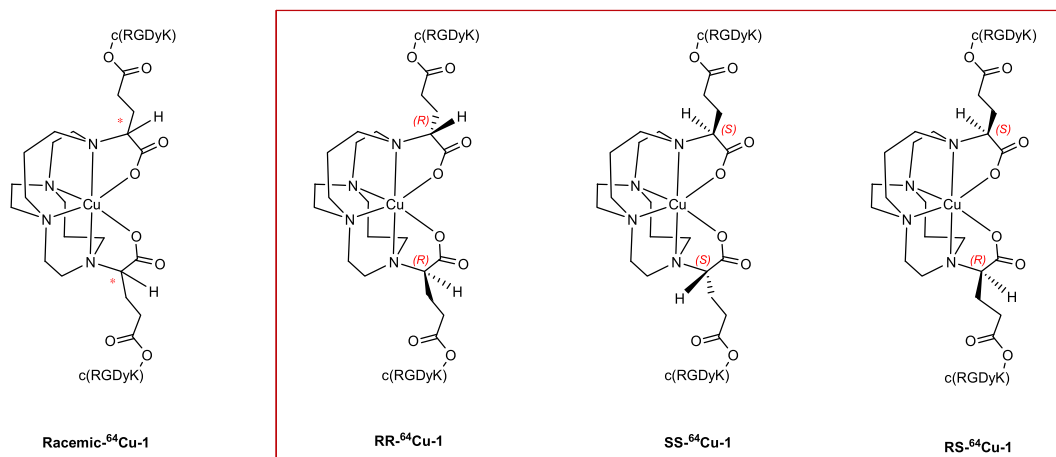
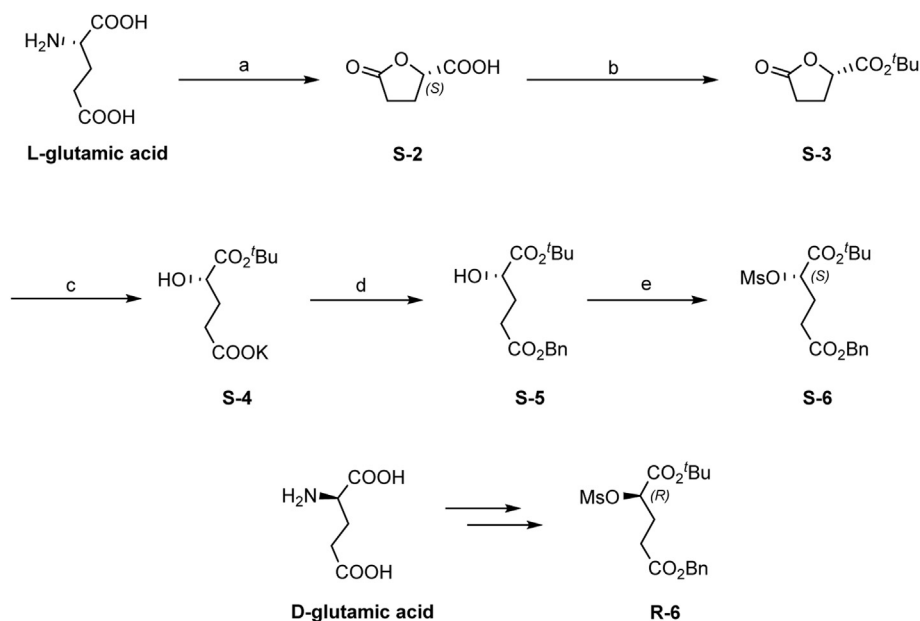
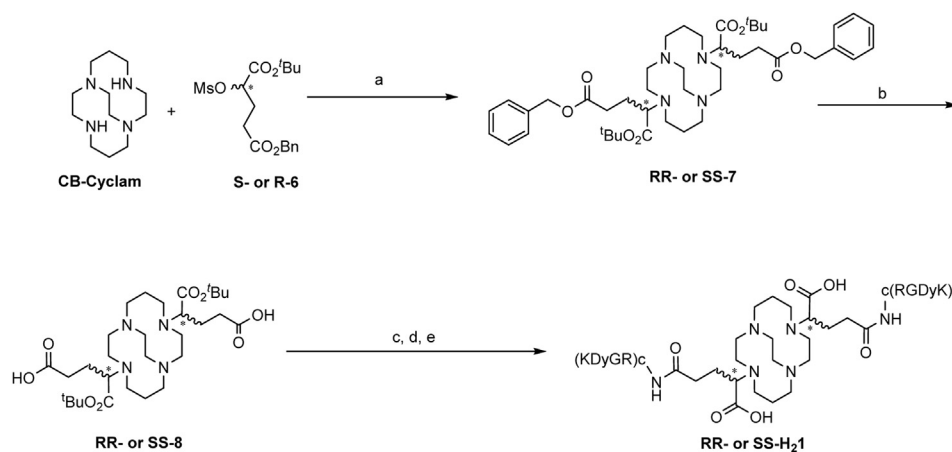


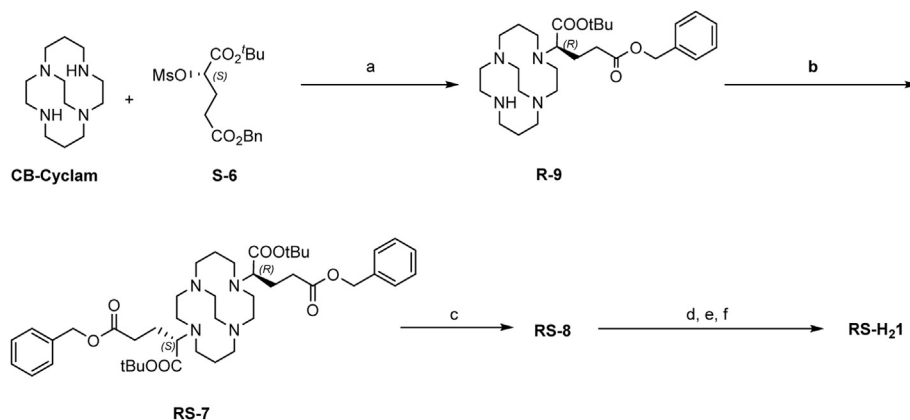
Fig. 1. Structures of peptide conjugates: rac- ^{64}Cu -1, RR- ^{64}Cu -1, SS- ^{64}Cu -1 and RS- ^{64}Cu -1.



Scheme 1. Synthesis of 5-benzyl 1-(*tert*-butyl) 2-((methylsulfonyl)oxy)pentadioate (**S-6**) and (**R-6**). Reagents and conditions: a) L-glutamic acid (1 equiv), HCl_{conc} , NaNO_2 (1.5 equiv), $\text{H}_2\text{O}/\text{dioxane}$, 0°C then r.t., 20 h; b) *t*-BuOH (1.1 equiv), DMAP (0.4 equiv), DCC (1.1 equiv), CH_2Cl_2 , r.t., 18 h; c) 1 N KOH (2 equiv), THF, 0°C then r.t., 4 h; d) BnBr (1 equiv), DMF, r.t., 8 h; e) MsCl (1.01 equiv), Et_3N (1.4 equiv), CH_2Cl_2 , 0°C then r.t., 2 h.



Scheme 2. Synthesis of **RR-H₂-1** and **SS-H₂-1**. Reagents and conditions: a) K_2CO_3 (1.2 equiv), CH_3CN , r.t. 24 h then 50°C 24 h; b) 10% Pd/C (catalytic), H_2 , 2-propanol, r.t. 12 h; c) NHS (4 equiv), EDC HCl (4 equiv), CH_3CN , r.t. 18 h; d) c(RGDyK) (4 equiv), DIPEA, DMF, r.t. 24 h; e) TFA, r.t. 12 h.



Scheme 3. Synthesis of **RS-H₂-1**. Reagents and conditions: a) K_2CO_3 (1.2 equiv), CH_3CN , r.t. 24 h then 50°C 24 h; b) **R-6** (1.5 equiv), K_2CO_3 (1.2 equiv), CH_3CN , r.t. 24 h then 50°C 24 h; c) 10% Pd/C (catalytic), H_2 , 2-propanol, r.t. 12 h; d) NHS (4 equiv), EDC HCl (4 equiv), CH_3CN , r.t. 18 h; e) c(RGDyK) (4 equiv), DIPEA, DMF, r.t. 24 h; f) TFA, r.t. 12 h.

yield. Addition of the chiral side arms, **S-6** and **R-6**, provided the BFC scaffolds **RR-7** and **SS-7**, respectively, with the complete inversion of configuration. The BFC scaffold **RS-7** was synthesized in two steps: reaction of CB-cylam with **S-6**, to yield scaffold **R-9**, followed by alkylation with **R-6** to provide **RS-7** in 40% yield.

The synthesized BFC scaffolds **RR-7**, **SS-7**, and **RS-7** contain two protected carboxylate groups at α and γ positions of the side arms. The benzyl protected γ -carboxylate groups were selectively deprotected and the resulting acids were conjugated with the c(RGDyK) peptide. Catalytic debenzoylation of **RR-7**, **SS-7**, and **RS-7** was achieved using 10% Pd/C in 2-propanol under hydrogen atmosphere to afford **RR-8**, **SS-8**, and **RS-8** in quantitative yield. The obtained γ -carboxylic acids were activated by N-hydroxysuccinimide (NHS) for acid-amine conjugation chemistry. The conjugation of NHS-activated **RR-8**, **SS-8**, and **RS-8** with two equivalents of c(RGDyK) in the presence of N, N-diisopropylethylamine (DIPEA) provided the *t*-butyl protected conjugates in quantitative yield. Finally, the α -carboxylate groups were deprotected using 95% trifluoroacetic acid to provide **RR-H₂-1**, **SS-H₂-1**, and **RS-H₂-1**, each of which contains two free carboxylic acids for radio-labeling with ^{64}Cu .

Compounds, **S-2** or **R-2** to **S-6** or **R-6** were characterized by ^1H and ^{13}C NMR and found to be identical to those reported in the literature [17]. Compounds, **S-2** or **R-2** to **S-6** or **R-6**, showed no differences in ^1H and ^{13}C NMR spectra as expected for enantiomers. The peptide conjugates were characterized by their molecular ion peak shown on MALDI-mass spectra, and the purity of the conjugates was verified by HPLC. Optical rotation $[\alpha]_D$ for compounds **RR-7** and **SS-7** was recorded to be +34.594 and –36.594 respectively, verifying that these compounds are enantiomers. Furthermore, the circular dichroism (CD) spectra measured in $\text{CH}_3\text{CN}:\text{H}_2\text{O}$ (1:5) solution, further confirm the enantiomeric nature of the optically active BFC scaffolds, **RR-8** and **SS-8**. The CD spectrum of **RR-8** shows a positive Cotton effect in the 230–280 nm region, while **SS-8** exhibits the opposite sign of the effect in the same range (Fig. 2).

2.2. Radiochemistry

All peptide conjugates (**rac-H₂-1**, **RR-H₂-1**, **SS-H₂-1**, and **RS-H₂-1**) were successfully labeled (>90% RCY) with ^{64}Cu within 30 min at 75 °C in 0.4 mM NH_4OAc buffer to provide **rac- ^{64}Cu -1**, **RR- ^{64}Cu -1**, **SS- ^{64}Cu -1**, and **RS- ^{64}Cu -1**, respectively. A series of radiolabeling conditions by decreasing the amount of peptide conjugates while the radioactivity of ^{64}Cu was fixed were tested to reach around 20 GBq/mmol specific activity. The ^{64}Cu -labeled conjugates were

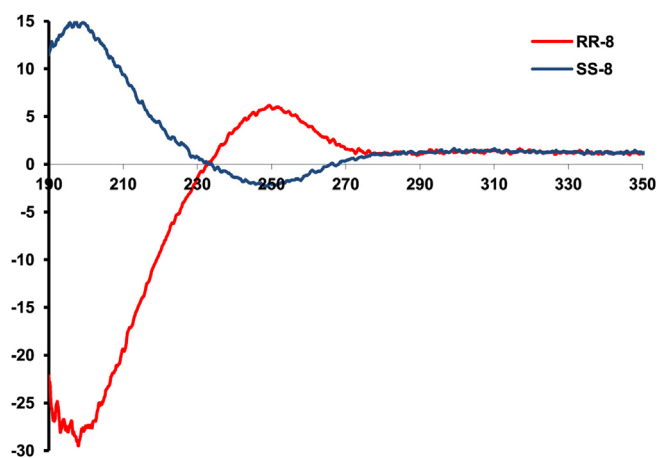


Fig. 2. Measured CD spectra of **RR-8** and **SS-8** in $\text{CH}_3\text{CN}:\text{H}_2\text{O}$ 1:5.

purified in one step using a pre-conditioned C-18 Sep-Pak light cartridge with a >90% recovery rate. The radiochemical purity of the ^{64}Cu -labeled conjugates after cartridge purification was >97% as determined by radio-HPLC. The overall radiochemical procedure including the synthesis and purification steps took less than 45 min.

2.3. Binding assay

The $\alpha_v\beta_3$ binding affinities of **rac-H₂-1**, **RR-H₂-1**, **SS-H₂-1**, and **RS-H₂-1** were measured by a competitive cell-binding assay using U87MG cells in which ^{125}I -echistatin was employed as $\alpha_v\beta_3$ -specific radioligand for competitive displacement. The U87MG cell line was chosen because the $\alpha_v\beta_3$ integrin density on the cell surface is the highest among the solid tumor cell lines that have been assessed [18]. The IC_{50} values of **rac-H₂-1**, **RR-H₂-1**, **SS-H₂-1**, and **RS-H₂-1** which represent their concentrations required to displace 50% of the ^{125}I -echistatin bound on the U87MG cells, were determined to be 106, 108, 85 and 100 nM, respectively ($n = 4$) with all p values >0.05 (see Fig. 3).

2.4. Small animal PET-CT imaging

To evaluate the effect of the chirality of BFC on the *in vivo* properties of the $\alpha_v\beta_3$ -targeted imaging agents, a comparative PET/CT imaging study was performed in SCID mice bearing integrin $\alpha_v\beta_3$ -positive PC-3 prostate cancer xenografts on a Siemens Inveon PET/CT Multimodality System. Representative trans-axial PET/CT images at 1, 4, and 24 h p.i. are displayed in Fig. 4. The PC-3 tumors were clearly visualized by all four probes up to 24 h p.i. The four agents showed nearly identical tumor uptake at the three time points, namely 2.72 ± 0.45 , 2.60 ± 0.52 , 2.45 ± 0.48 and 2.88 ± 0.59 for **rac- ^{64}Cu -1**, **RR- ^{64}Cu -1**, **SS- ^{64}Cu -1**, and **RS- ^{64}Cu -1** respectively at 1 h p.i., 2.32 ± 0.37 , 2.13 ± 0.49 , 1.58 ± 0.32 and 1.73 ± 0.36 at 4 h p.i. and 1.77 ± 0.32 , 1.92 ± 0.51 , 1.16 ± 0.20 and 1.22 ± 0.31 at 24 h p.i. with all p values > 0.05 except for **SS- ^{64}Cu -1** that showed significantly lower uptake than other conjugates at 4 and 24 h p.i. due to its lower specific activity at the injection time. In addition, we compared their *in vivo* distribution profiles in major organs and

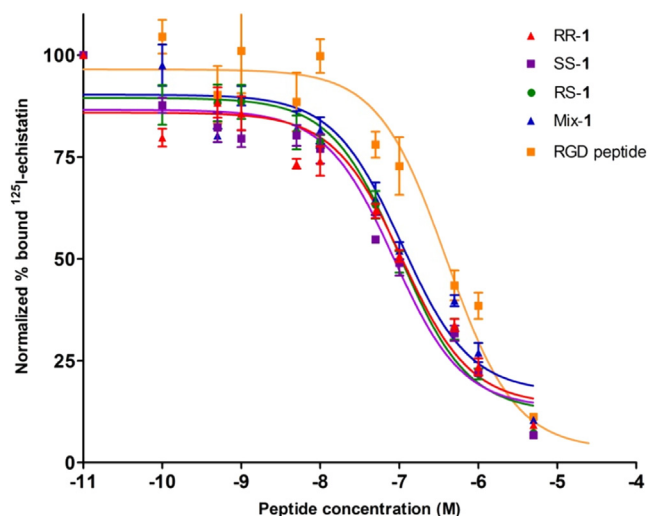


Fig. 3. The integrin $\alpha_v\beta_3$ binding affinities of cRGDyK peptide, **RR-1**, **SS-1**, **RS-1** and **rac-1** measured by a competitive cell-binding assay using ^{125}I -echistatin as the radioligand. The IC_{50} values were calculated to be 396 nM (cRGDyK), 108 nM (**RR-1**), 85 nM (**SS-1**), 100 nM (**RS-1**) and 106 nM (**rac-1**) (R^2 : 0.91–0.94).

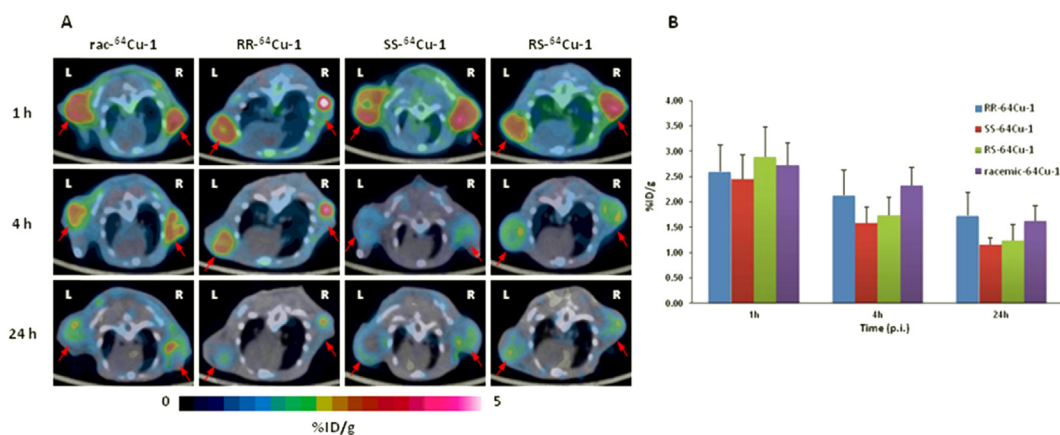


Fig. 4. (A) Comparative transaxial PET/CT images of PC-3 tumors in SCID mice intravenously injected with rac-⁶⁴Cu-1, RR-⁶⁴Cu-1, SS-⁶⁴Cu-1, and RS-⁶⁴Cu-1 at 1 h, 4 h, and 24 h p.i. (B) Quantitative tumor uptake analysis of the four ⁶⁴Cu-labeled peptide conjugates (n = 6).

found that the stereoisomers shared a similar biodistribution pattern in the mouse tumor model.

3. Discussion

Copper has several radioisotopes of interest for the development of radiopharmaceuticals, which can be used for PET imaging (⁶¹Cu, ⁶²Cu, and ⁶⁴Cu) and radiotherapy (⁶⁴Cu and ⁶⁷Cu). Most copper radiopharmaceuticals are designed and prepared by incorporation of copper radioisotope into a biological substrate through the linkage often provided by a tetraazamacrocyclic BFC [6,7,19,20]. The BFCs usually consist of a Cu(II) chelating moiety and a pendent linker for the attachment to a biomolecule of interest. As such, the carbon atoms in the pendent linker may become chiral depending on the chemical modification as in our reported design of CB-TE2GA. In the case of drugs, these subtle stereo chemical differences may lead to one form of the chiral molecule being therapeutically beneficial, while the other form may be physiologically neutral or even harmful [21,22]. However, very little information is available on stereoisomerism of the radiolabeled macrocyclic BFC-conjugate at tracer level [23–25].

The role of linker chirality on ligand-receptor interaction partially depends upon the application of the linker. In case of monovalent BFC, where linker is solely used as the attachment point, the linker chirality is not supposed to play significant role in ligand-receptor interaction. This is clearly exemplified by ^{99m}Tc-(HYNIC-K(NIC)-3G-RGD₂) (tricine) monovalent conjugates, where no significant differences in biological behavior or properties were observed for its separable enantiomers or diastereomers [23]. The results for the monovalent conjugates are not surprising given the fact that one radioligand binds to one receptor site, which perhaps is the main reason that the commercial available BFCs, such as DOTA-SCN and NOTA-SCN, are provided as racemates. In the case of multivalent BFC, multiple linkers provide multiple attachment points as well as different spatial orientations for the multi-presentation of a biologically active molecule, where the linker chirality may play a significant role in multi-valent or multiplexing ligand-receptor interactions.

In our reported multivalent BFC scaffold design for ⁶⁴Cu-based PET imaging probe, the BFC scaffold provides multiple peripheral functional points for multi-presentation of targeting vectors. Bearing two chiral carbon atoms in the glutaric acid side arm, the BFC scaffold can have three potential stereoisomers RR-**8**, SS-**8**, and RS-**8** [14,15]. Attachment of c(RGDyK) to the chiral side arms leads to different spatial dispositions of the c(RGDyK) depending on the

chirality of the side arms, which can potentially impact their binding affinities to the target receptors. Indeed it was reported that, when two binding motifs of gonadotropin-releasing hormone (GnRH) peptide (intact peptide: pEHWSYGLRPG-NH₂, binding motifs: pEHW and RPG) were connected by D-Lys or L-Lys, a difference of more than two orders of magnitude was observed in their binding to GnRH receptor [25]. Therefore we reasoned that the enantiopure peptide conjugates (RR-H₂-1, SS-H₂-1, RS-H₂-1) might yield different ligand-receptor affinity and hence *in vivo* properties of the corresponding copper radiopharmaceuticals.

Synthesis of the enantiopure side arms was the key step towards the success of this work. Enantiopure side arms, R-**6** and S-**6**, were synthesized in gram quantity from D/L-glutaric acid, respectively [16]. The enantio-selective synthesis relied on the use of an enantio-specific deamination reaction to form the lactone (Scheme 1). Further functionalization of the lactone, as well as the ring opening reaction does not affect the conformation of the molecule. The synthesis of BFC scaffolds, RR-**7**, and SS-**7**, was achieved in one step by dialkylation of CB-cyclam using enantiopure side arm, S-**6**, and R-**6**, respectively. On the other hand, for the synthesis of RS-**7**, stepwise alkylation was required using different enantiomer in each step. The alkylation of CB-cyclam proceeded via an S_N2 type reaction to provide the product with inversion of configuration. Finally, RR-H₂-1, SS-H₂-1, and RS-H₂-1 were synthesized by conjugating the c(RGDyK) peptide with the outer carboxylate groups, followed by deprotection of the inner carboxylate groups using 95% TFA for radiolabeling with copper radioisotopes.

The designed imaging agents, enantiopure (RR-⁶⁴Cu-1, SS-⁶⁴Cu-1) and the meso (RS-⁶⁴Cu-1) contain two c(RGDyK) units for multivalent interactions. The distance between the two RGD motifs in the conjugates is greater than 25 bonds (including the lysine spacers), the minimum spacing length required to realize multivalent binding of RGD motifs to the α_vβ₃ integrin [26]. The spatial orientations of the c(RGDyK) units are expected to be different in each stereoisomeric conjugate. To evaluate the chirality effect of BFC on the imaging properties of the agents, we performed PET/CT imaging in PC-3 tumor bearing mice. To our surprise, all the agents showed similar bio-distribution and tumor uptake at all-time points. This observation suggests that the spatial orientation difference of the two c(RGDyK) units presented on the chiral BFC scaffold has negligible effects on the bio-distribution profile of the α_vβ₃-targeted imaging agents in the mouse tumor model. This may indicate that the multivalent ligand-receptor interaction is likely a stepwise mechanism. Since the multivalent binding can be a concerted process, binding of one RGD unit to integrin α_vβ₃ enables

the second RGD unit to reorient itself towards a second $\alpha_v\beta_3$ binding site as long as the spacer between them including the chelator moiety is flexible. However, given the fact that ligand–receptor interaction is receptor specific, what we have observed with the chiral BFC scaffolds for integrin $\alpha_v\beta_3$ in this work may not be necessarily conserved for other receptors. Judicious selection of BFC scaffolds with regards to their chirality should still be considered so as to achieve the optimal imaging properties for noninvasive assessment of the expression status of specific biomarkers towards personalized disease stratification.

4. Conclusions

Three enantiopure BFC scaffolds for copper radiopharmaceuticals were designed and synthesized. Using well-validated integrin $\alpha_v\beta_3$ ligand, c(RGDyK), peptide conjugates of the enantiopure BFC scaffolds were prepared to evaluate the effect of BFC chirality on ligand–receptor binding and the implications on the *in vivo* behavior of so-designed agents. Our work suggests that the chirality of BFC scaffolds plays an insignificant role in integrin $\alpha_v\beta_3$ targeted copper radiopharmaceuticals. Although this observation does not support our design rationale, the importance of BFC chirality in radiopharmaceutical agents cannot be undervalued without discretion when it is applied to other biological targets.

5. Experimental section

5.1. General methods and materials

All reactions were carried out under N_2 atmosphere in degassed dried solvents. Commercially available starting materials were purchased from vendors and used directly without further purification unless otherwise stated. Milli-Q water (18 M Ω cm) was obtained from a Millipore Gradient Milli-Q water system (Billerica, MA). All aqueous solutions were prepared with Milli-Q water. Silica gel 60 (70–230 mesh, Merck) was used for column chromatography. Analytical thin-layer chromatography (TLC) was performed using F254 silica gel (precoated sheets, 0.2 mm thick) (Lawrence, KS). 1H and ^{13}C NMR spectra were recorded on a Varian 400 spectrometer; chemical shifts are expressed in ppm relative to TMS (0.0 ppm). Matrix-assisted laser desorption/ionization (MALDI) mass spectra were acquired on an Applied Biosystems Voyager-6115 mass spectrometer. Optical rotation data were collected on a APIV-6W Rudolph Research automatic polarimeter. Radiolabeled conjugates were purified by Light C-18 Sep-Pak cartridges (Waters, Milford, MA).

Bulk solvents were removed by rotary evaporator under reduced pressure, and trace solvents were removed by vacuum pump. 1,4,8,11-tetraazabicyclo[6.6.2]hexadecane (CB-cyclam) was synthesized according to a published procedure [27]. $^{64}Cu(II)$ in 0.1 M HCl was purchased from either Washington University School of Medicine in St. Louis or the University of Wisconsin at Madison.

5.2. High performance liquid chromatography (HPLC) methods

HPLC separation was performed on a Waters 600 Multisolute Delivery System equipped with a Waters 2996 Photodiode Array detector. The mobile phase consisted of H_2O with 0.1% TFA (solvent A) and acetonitrile with 0.1% TFA (solvent B). The analytical HPLC was performed on an XTerra RP18 column (150 \times 4.6 mm) with a gradient of 0% B to 100% B in 50 min at the flow rate of 1.0 mL/min. The HPLC separation was performed on a semi-preparative XTerra RP18 Column (250 \times 10 mm) with a gradient of 0% B to 100% B in 50 min at the flow rate of 4.0 mL/min.

5.3. Integrin $\alpha_v\beta_3$ binding assay

The binding affinities of c(RGDyK), rac-H₂-1, RR-H₂-1, RS-H₂-1, and SS-H₂-1 to integrin $\alpha_v\beta_3$ were determined by a competitive cell-binding assay using ^{125}I -echistatin (PerkinElmer) as the $\alpha_v\beta_3$ -specific radioligand. The experiments were performed on U87MG human glioblastoma cells following our previously reported method [10]. Briefly, U87MG cells were grown in RPMI 1640 medium supplemented with penicillin, streptomycin, and 10% (v/v) fetal bovine serum (FBS) at 37 °C under 5% CO_2 . Suspended U87MG cells in binding buffer (20 mM Tris, pH 7.4, 150 mM NaCl, 2 mM $CaCl_2$, 1 mM $MgCl_2$, 1 mM $MnCl_2$, 0.1% bovine serum albumin) were seeded on multi-well DV plates (Millipore) with 5×10^4 cells per well and then incubated with ^{125}I -echistatin (10,000 cpm/well) in the presence of increasing concentrations (0–5000 nM) of c(RGDyK) peptide conjugates for 2 h. The final volume in each well was maintained at 250 μ L. At the end of incubation, unbound ^{125}I -echistatin was removed by filtration followed by five rinses with cold binding buffer. The retentive was collected and the radioactivity was measured using a γ -counter. The best-fit IC_{50} values (inhibitory concentration where 50% of the ^{125}I -echistatin bound on U87MG cells are displaced) of c(RGDyK), rac-H₂-1, RR-H₂-1, SS-H₂-1, and RS-H₂-1 were calculated by fitting the data with nonlinear regression using GraphPad Prism (GraphPad Software, Inc.). Experiments were duplicated with quintuplicate samples.

5.4. Tissue culture and animal model

All animal studies were performed in compliance with guidelines set by the UT Southwestern Institutional Animal Care and Use Committee (IACUC). The PC-3 cell line was obtained from the American Type Culture Collection (ATCC, Manassas, VA), and was cultured in T-media (Invitrogen, Carlsbad, CA) at 37 °C in an atmosphere of 5% CO_2 and were passaged at 75% confluence in P150 plates. T-media was supplemented with 5% Fetal Bovine Serum (FBS) and 1 \times Penicillin/Streptomycin. PC-3 cells were harvested from monolayer using PBS and trypsin/EDTA, and suspended in T-media with 5% FBS. The cell suspension was then injected subcutaneously (5×10^5 cells in 100 μ L media) into the front flanks of male SCID (Severe combined immunodeficiency) mice. After injection, animals were monitored three times a week by general observations. The tumor was allowed to grow three weeks to reach a palpable size (50–150 mm³) for microPET/CT imaging studies.

5.5. Mouse PET/CT imaging

The imaging studies were performed on a Siemens Inveon Multimodality PET/CT system once the tumor size reached the range of 50–150 mm³ (tumor volume = $\frac{1}{2}$ (length \times width²)). One hour prior to imaging, each mouse bearing PC-3 tumor was injected with 100–125 μ Ci of a ^{64}Cu labeled conjugate in 100 μ L of saline via the tail vein. Ten minutes prior to imaging, the animals were anesthetized using 3% isoflurane at room temperature until stable vitals were established. Once the animal was sedated, it was placed onto the imaging bed under 2% isoflurane anesthesia for the duration of imaging data requisition. At each time point (1 h, 4 h, and 24 h) post-injection (p.i.), a CT scan was performed (8 min), followed immediately by a static PET scan (15 min). The CT imaging was acquired at 80 kV and 500 μ A with a focal spot of 58 μ m. The total rotation of the gantry was 360° with 360 rotation steps obtained at an exposure time of approximately 180 ms/frame. The images were attained using CCD readout of 4096 \times 3098 with a binning factor of four and an average frame of one. Under low magnification the effective pixel size was 103.03 μ m. The CT images were reconstructed with a down sample factor of two using Cobra

Reconstruction Software. PET images were reconstructed using Fourier Rebinning and Ordered Subsets Expectation Maximization 3D (OSEM3D) algorithm. Reconstructed CT and PET images were fused and analyzed using the manufacturer's software. For quantification, regions of interest were placed in the areas expressing the highest ^{64}Cu -labeled conjugate activity as determined by PET and visually guided by CT images. The tissues examined include the tumor, heart, liver, lung, kidney, and muscle. The resulting quantitative data were expressed in percentage of the injected dose in per gram of the tissue (%ID/g) on the assumption that the density of the tissue is 1 g/cm^3 .

5.6. Synthesis

5.6.1. Synthesis of (S)-5-oxotetrahydrofuran-2-carboxylic acid (S-2)

L-glutamic acid (30.0 g, 200 mmol) was suspended in a water/dioxane mixture (75/25 mL) and stirred at $0\text{ }^\circ\text{C}$ for 30 min. The white slurry became clear after 40 mL of concentrated HCl (37%) was added, followed by drop-wise addition of a solution of NaNO_2 (21.0 g, 300 mmol) in 50 mL of water. The reaction temperature was maintained around $0\text{ }^\circ\text{C}$ during the 4 h of addition. The reaction mixture was then left stirring at room temperature for 20 h. Upon completion, the solvent was evaporated under reduced pressure to provide a white solid, which was then treated with EtOAc (300 mL) and Na_2SO_4 for 30 min. The solution was filtered and the solvent was evaporated to yield S-2 as a white solid (21.50 g, 78%). $^1\text{H NMR}$ (400 MHz, CDCl_3) δ 11.08 (bs, 1H), 5.01 (m, 1H), 2.71–2.55 (m, 3H), 2.45–2.37 (m, 1H); $^{13}\text{C NMR}$ (100 MHz, CDCl_3) δ 176.8, 174.5, 75.4, 26.8, 25.7.

5.6.2. Synthesis of tert-butyl (S)-5-oxotetrahydrofuran-2-carboxylate (S-3)

In a solution of S-2 (10.0 g, 77 mmol) in CH_2Cl_2 (240 mL), *t*-butanol (8 mL, 84 mmol) and 4-dimethylaminopyridine (DMAP, 3.75 g, 31 mmol) were added and the reaction mixture was cooled to $0\text{ }^\circ\text{C}$. To this solution, *N,N*-dicyclohexylcarbodiimide (DCC, 16.2 g, 84.5 mmol) in CH_2Cl_2 (80 mL) was added dropwise. The reaction was stirred at room temperature overnight and upon completion the solvent was removed under reduced pressure. The residue was purified by column chromatography (silica gel, gravity) using hexane (250 mL) and EtOAc:hexane (1:4) to give S-3 as white solid (7.0 g, 55%): $^1\text{H NMR}$ (400 MHz, CDCl_3) δ 4.79 (m, 1H), 2.65–2.44 (m, 3H), 2.24 (m, 1H), 1.48 (s, 9H) ppm; $^{13}\text{C NMR}$ (100 MHz, CDCl_3) δ 176.2, 169.0, 83.1, 76.2, 27.9, 26.8, 25.8 ppm.

5.6.3. Synthesis of potassium (S)-5-(tert-butoxy)-4-hydroxy-5-oxopentanoate (S-4)

Compound S-3 (5.0 g, 30 mmol) was dissolved in THF (60 mL), and cooled to $0\text{ }^\circ\text{C}$. To this mixture, 1 N KOH (aqueous, 66 mL) was added dropwise. The resulting mixture was stirred at room temperature over 4 h and upon completion the solvent was evaporated to give S-4 as white solid. Compound S-4 was directly used for the synthesis of S-5. However, for characterization of the compound, a sample of S-4 was converted to its acid using 3 N hydrochloric acid. The acidified aqueous layer was then extracted with EtOAc ($3 \times 30\text{ mL}$). The organic layers were combined and dried over anhydrous MgSO_4 and concentrated. The residue was purified by column chromatography (silica gel, gravity) using hexane (100 mL) and EtOAc:hexane (1:3) to yield the acid form of S-4 as a white solid (3.0 g, 60%): $^1\text{H NMR}$ (400 MHz, CDCl_3) δ 4.10 (m, 1H), 2.57–2.41 (m, 2H), 2.16–2.07 (m, 1H), 1.92–1.83 (m, 1H), 1.47 (s, 9H); $^{13}\text{C NMR}$ (100 MHz, CDCl_3) δ 178.6, 173.9, 82.8, 69.5, 29.4, 29.0, 27.8.

5.6.4. Synthesis of 5-benzyl 1-(tert-butyl) (S)-2-hydroxypentanedioate (S-5)

S-4 (2.0 g, 9.8 mmol) was suspended in DMF (15 mL), to which was added benzyl bromide (1.67 g, 9.8 mmol). After stirred for 8 h, the mixture was poured into ice water (20 mL) and extracted with EtOAc ($3 \times 25\text{ mL}$). The combined organic layer was dried over Na_2SO_4 and concentrated under reduced pressure. The residue was purified by column chromatography (silica gel, gravity) using hexane and EtOAc:hexanes (1:4) to give S-5 as a white solid (1.5 g, 52%). $^1\text{H NMR}$ (400 MHz, CDCl_3) δ 7.35 (m, 5H), 5.13 (s, 2H), 4.08 (bs, 1H), 2.88 (bs, 1H), 2.59–2.44 (m, 2H), 2.17 (m, 2H), 1.91 (m, 1H), 1.48 (s, 9H). $^{13}\text{C NMR}$ (100 MHz, CDCl_3) δ 173.9, 173.0, 135.9, 128.5, 128.2, 128.1, 82.8, 69.6, 66.3, 29.7, 29.4, 28.0.

5.6.5. Synthesis of 5-benzyl 1-(tert-butyl) (S)-2-((methylsulfonyl)oxy)pentanedioate (S-6)

Methanesulfonyl chloride (0.42 g, 3.7 mmol) was added to a mixture of S-5 (1.0 g, 3.4 mmol) and Et_3N (0.47 g, 4.7 mmol) in CH_2Cl_2 (25 mL) at $0\text{--}5\text{ }^\circ\text{C}$. After the addition was completed, the mixture was warmed to room temperature and stirred for 2 h. Upon completion, water (10 mL) was added, the organic phase was separated and washed with brine ($3 \times 10\text{ mL}$), dried over Na_2SO_4 and concentrated to give S-6 (0.7 g, 60%). $^1\text{H NMR}$ (400 MHz, CDCl_3) δ 7.36 (m, 5H), 5.14 (s, 2H), 4.98 (m, 1H), 3.11 (s, 3H), 2.55 (m, 2H), 2.30 (m, 1H), 1.49 (s, 9H). $^{13}\text{C NMR}$ (100 MHz, CDCl_3) δ 171.8, 167.4, 135.5, 128.5, 128.2, 128.2, 83.5, 76.6, 66.5, 38.9, 29.3, 27.8, 27.0.

The synthesis of 5-benzyl 1-(tert-butyl) (R)-2-((methylsulfonyl)oxy)pentanedioate (R-6) was accomplished in the same way as above from D-glutamic acid.

5.6.6. Synthesis of compound RR-7

Compound S-6 (500 mg, 1.3 mmol) was added to a suspension of cross-bridge cyclam (150 mg, 0.6 mmol) and K_2CO_3 (0.10 g) in anhydrous acetonitrile (50 mL). The reaction was stirred at room temperature for 24 h and then for another 24 h at $50\text{ }^\circ\text{C}$. The reaction mixture was filtered and the solid was washed twice with chloroform ($2 \times 20\text{ mL}$). The combined filtrates were concentrated under reduced pressure and purified by column chromatography (silica gel, 60–230 mesh) using 10:1 $\text{CHCl}_3/\text{MeOH}$ to 9:1 EtOAc/isopropylamine to yield RR-7 as viscous oil (250 mg; Yield: 52%); MALDI-TOF/MS [M^+]: calc': 778.49; found: 778.59.

5.6.7. Synthesis of compound RR-H₂1

To a solution of RR-7 (13 mg, 16.7 μmol) in 0.5 mL of 2-propanol was added portion wise 10 mg of 10% Pd/C. The suspension was shaken in a hydrogenator (Parr, Moline, Illinois) at room temperature for 12 h under an H_2 atmosphere (60 psi). After removal of the solids, evaporation of the solvent afforded compound RR-8 as a white foam in nearly quantitative yield. A mixture of compound RR-8 (10.0 mg, 16.7 μmol), *N*-hydroxysuccinimide (7.6 mg, 66.8 μmol) and EDC·HCl (12.8 mg, 66.8 μmol) in 500 μL of dry acetonitrile (MeCN) was stirred under N_2 for overnight. The solvent was removed under reduced pressure and the residue was redissolved in CHCl_3 (1 mL) and then washed with water promptly three times ($3 \times 2\text{ mL}$). CHCl_3 was evaporated under reduced pressure, the residue was frozen by liquid nitrogen and the remaining water was removed by a freeze dryer to give a pale yellow solid in quantitative yield. The activated ester was used directly for the next reaction without further purification. Cyclic Arg-Gly-Asp-D-Tyr-Lys [c(RGDyK)] (10 mg, 16 μmol) was mixed with the activated ester (2.4 mg, 4 μmol) in 200 μL of anhydrous DMF. To this solution, 30 μL of *N,N*-diisopropylethylamine (DIPEA) were added. The mixture was stirred at room temperature for 24 h under N_2 . Upon completion, the solvent was evaporated under reduced pressure and the crude product was purified by HPLC. The collected fractions

were combined and lyophilized to yield the *t*-butyl protected product, which was then dissolved in 95% TFA and stirred at room temperature for 12 h. After evaporation of the solvent, the residue was purified by semi-preparative reverse-phase HPLC. The collected fractions from multiple runs were collected and lyophilized to afford RR-H₂1 as white solid at quantitative yield. MALDI-TOF/MS [M+H⁺]: calc'd: 1689.87; found: 1690.67.

5.6.8. Synthesis of compound SS-H₂1

Compound SS-H₂1 was synthesized in a similar manner starting from CB-Cyclam and R-6. MALDI-TOF/MS [M+H⁺]: calc'd: 1689.87; found: 1690.67.

5.7. Radiolabeling of *rac*-H₂-1, *RR*-H₂-1, *RS*-H₂-1, and *SS*-H₂-1 with ⁶⁴Cu

To a 1.5 mL vial containing 5 μg of respective conjugate in 200 μL of 0.4 M NH₄OAc (pH = 6.5) solution, 2–3 mCi of ⁶⁴Cu(II) in 0.1 M HCl were added. The reaction mixture was shaken and incubated at 75 °C for 0.5 h. Then, 5 μL of 5 mM diethylenetriaminepentaacetic acid (DTPA) was added into the reaction mixture and allowed to incubate for another 5 min. After incubation, purification of ⁶⁴Cu-labeled conjugate was carried out by passing the mixture through a preconditioned Sep-Pak C-18 light cartridge. After thorough rinsing (3 × 3 mL water) of the cartridge, the ⁶⁴Cu-labeled conjugate was eluted by an ethanol-water mixture (70:30). Radio-TLC analysis was performed on a Rita Star Radioisotope TLC Analyzer (Straubenhardt, Germany) to monitor the radiolabeling efficiency via ITLC paper, developed by 10 mM PBS. High performance liquid chromatography (HPLC) analysis was conducted to determine radiochemical purity of the products on a Waters 600 Multisolute Delivery System equipped with a Waters 2996 Photodiode Array (PDA) detector and an in-line Shell Jr. 2000 radio-detector (Fredericksburg, VA) on a Waters Xtera column (150 × 4.6 mm, 5 μm). The gradient mobile phase started with 100% A (0.1% TFA in H₂O) to 50% B (0.1% TFA in MeCN) and 50% A at 25 min with a flow rate of 1 mL/min.

5.8. Statistical analysis

Quantitative data were expressed as the mean ± SD. Unpaired *t* test (two-tailed, confidence intervals: 95%) was performed using GraphPad Prism. *P* values of <0.05 were considered statistically significant.

Conflict of interests

The authors declare no conflicts of interest.

Appendix A. Supplementary data

Supplementary data related to this article can be found at <http://dx.doi.org/10.1016/j.ejmech.2014.04.071>.

References

- [1] R.T.M. de Rosales, E. Arstad, P.J. Blower, Nuclear imaging of molecular processes in cancer, *Targeted Oncology* 4 (2009) 183–197.
- [2] S.S. Gambhir, Molecular imaging of cancer with positron emission tomography, *Nature Reviews. Cancer* 2 (2002) 683–693.
- [3] V.N. Harry, S.I. Semple, D.E. Parkin, F.J. Gilbert, Use of new imaging techniques to predict tumour response to therapy, *The Lancet Oncology* 11 (2010) 92–102.
- [4] G. Kelloff, J.M. Hoffman, B. Johnson, H.I. Scher, B.A. Siegel, E.Y. Cheng, B.D. Cheson, J. O'Shaughnessy, K.Z. Guyton, D.A. Mankoff, L. Shankar, S.M. Larson, C.C. Sigman, R.L. Schilsky, D.C. Sullivan, Progress and promise of FDG-PET imaging for cancer patient management and oncologic drug development, *Clinical Cancer Research* 11 (2005) 2785–2808.
- [5] G.K. von Schulthess, H.C. Steinert, T.F. Hany, Integrated PET/CT-3: current applications and future directions, *Radiology* 238 (2006) 405–422.
- [6] G. Hao, A.N. Singh, W. Liu, X. Sun, PET with non-standard nuclides, *Current Topics in Medicinal Chemistry* 10 (2010) 1096–1112.
- [7] G. Hao, A.N. Singh, O.K. Oz, X. Sun, Recent advances in copper radiopharmaceuticals, *Current Radiopharmaceuticals* 4 (2011) 109–121.
- [8] R. Haubner, H.R. Wester, Radiolabeled tracers for imaging of tumor angiogenesis and evaluation of anti-angiogenic therapies, *Current Pharmaceutical Design* 10 (2004) 1439–1455.
- [9] R. Rossin, S. Muro, M.J. Welch, V.R. Muzyk, D.P. Schuster, In vivo imaging of Cu-64-labeled polymer nanoparticles targeted to the lung endothelium, *Journal of Nuclear Medicine* 49 (2008) 103–111.
- [10] W. Liu, G.Y. Hao, M.A. Long, T. Anthony, J.T. Hsieh, X.K. Sun, Imparting multivalency to a bifunctional chelator: a scaffold design for targeted PET imaging probes, *Angewandte Chemie International Edition* 48 (2009) 7346–7349.
- [11] X.K. Sun, M. Wuest, G.R. Weisman, E.H. Wong, D.P. Reed, C.A. Boswell, R. Motekaitis, A.E. Martell, M.J. Welch, C.J. Anderson, Radiolabeling and in vivo behavior of copper-64-labeled cross-bridged cyclam ligands, *Journal of Medicinal Chemistry* 45 (2002) 469–477.
- [12] K.S. Woodin, K.J. Heroux, C.A. Boswell, E.H. Wong, G.R. Weisman, W.J. Niu, S.A. Tomellini, C.J. Anderson, L.N. Zakharov, A.L. Rheingold, Kinetic inertness and electrochemical behavior of copper(II) tetraazamacrocyclic complexes: possible implications for in vivo stability, *European Journal of Inorganic Chemistry* (2005) 4829–4833.
- [13] C.A. Boswell, X.K. Sun, W.J. Niu, G.R. Weisman, E.H. Wong, A.L. Rheingold, C.J. Anderson, Comparative in vivo stability of copper-64-labeled cross-bridged and conventional tetraazamacrocyclic complexes, *Journal of Medicinal Chemistry* 47 (2004) 1465–1474.
- [14] J. Notni, J. Simecek, P. Hermann, H.J. Wester, TRAP, a powerful and versatile framework for gallium-68 radiopharmaceuticals, *Chemistry: A European Journal* 17 (2011) 14718–14722.
- [15] A.N. Singh, W. Liu, G.Y. Hao, A. Kumar, A. Gupta, O.K. Oz, J.T. Hsieh, X.K. Sun, Multivalent bifunctional chelator scaffolds for gallium-68 based positron emission tomography imaging probe design: signal amplification via multivalency, *Bioconjugate Chemistry* 22 (2011) 1650–1662.
- [16] R.C. Cooke, K.A. van Leeuwen, D.L. Capone, R. Gawel, G.M. Elsey, M.A. Sefton, Odor detection thresholds and enantiomeric distributions of several 4-alkyl substituted γ -lactones in Australian red wine, *Journal of Agricultural and Food Chemistry* 57 (2009) 2462–2467.
- [17] S.G. Levy, V. Jacques, K.L. Zhou, S. Kalogeropoulos, K. Schumacher, J.C. Amedio, J.E. Scherer, S.R. Witowski, R. Lombardy, K. Koppetsch, Development of a multigram asymmetric synthesis of 2-(R)-2-(4,7,10-Tris tert-Butylcarboxymethyl-1,4,7,10-tetraazacyclododec-1-yl)-pentanedioic acid, 1-tert-butyl ester (R)-tert-Bu-4-DOTAGA, *Organic Process Research & Development* 13 (2009) 535–542.
- [18] X.Z. Zhang, Z.M. Xiong, Y. Wu, W.B. Cai, J.R. Tseng, S.S. Gambhir, X.Y. Chen, Quantitative PET imaging of tumor integrin $\alpha(v)\beta(3)$ expression with F-18-FRGD2, *Journal of Nuclear Medicine* 47 (2006) 113–121.
- [19] C.J. Anderson, R. Ferdani, Copper-64 radiopharmaceuticals for PET imaging of cancer: advances in preclinical and clinical research, *Cancer Biotherapy and Radiopharmaceuticals* 24 (2009) 379–393.
- [20] M. Shokeen, C.J. Anderson, Molecular imaging of cancer with copper-64 radiopharmaceuticals and Positron Emission Tomography (PET), *Accounts of Chemical Research* 42 (2009) 832–841.
- [21] N.M. Davies, X.W. Teng, Importance of chirality in drug therapy and pharmacy practice: implications for psychiatry, *Advances in Pharmacy* 1 (2003) 242–252.
- [22] S.J. Gardiner, E.J. Begg, Pharmacogenetics, drug-metabolizing enzymes, and clinical practice, *Pharmacological Reviews* 58 (2006) 521–590.
- [23] Y. Zhou, Y.-S. Kim, X. Lu, S. Liu, Evaluation of ^{99m}Tc-labeled cyclic RGD Dimers: impact of cyclic RGD peptides and ^{99m}Tc chelates on biological properties, *Bioconjugate Chemistry* 23 (2012) 586–595.
- [24] F.L.G. Gomez, T. Uehara, T. Rokugawa, Y. Higaki, H. Suzuki, H. Hanaoka, H. Akizawa, Y. Arano, Synthesis and evaluation of diastereoisomers of 1,4,7-triazacyclononane-1,4,7-tris-(glutaric acid) (NOTGA) for multimeric radiopharmaceuticals of gallium, *Bioconjugate Chemistry* 23 (2012) 2229–2238.
- [25] H.X. Guo, J. Lu, H. Hathaway, M.E. Royce, E.R. Prossnitz, Y.B. Miao, Synthesis and evaluation of novel gonadotropin-releasing hormone receptor-targeting peptides, *Bioconjugate Chemistry* 22 (2011) 1682–1689.
- [26] Z.B. Li, W.B. Cai, Q.Z. Cao, K. Chen, Z.H. Wu, L.N. He, X.Y. Chen, ⁶⁴Cu-Labeled tetrameric and octameric RGD peptides for small-animal PET of tumor $\alpha(v)\beta(3)$ integrin expression, *Journal of Nuclear Medicine* 48 (2007) 1162–1171.
- [27] E.H. Wong, G.R. Weisman, D.C. Hill, D.P. Reed, M.E. Rogers, J.S. Condon, M.A. Fagan, J.C. Calabrese, K.-C. Lam, I.A. Guzei, A.L. Rheingold, Synthesis and characterization of cross-bridged cyclams and pendant-armed derivatives and structural studies of their copper(II) complexes, *Journal of the American Chemical Society* 122 (2000) 10561–10572.